

Auger Recombination Lifetime Scaling for Type-I and Quasi-Type-II Core/Shell Quantum Dots

John P. Philbin*

Department of Chemistry, University of California, Berkeley, California 94720, United States

Eran Rabani†

*Department of Chemistry, University of California, Berkeley, California 94720, United States
Materials Sciences Division, Lawrence Berkeley National Laboratory, Berkeley, California 94720, United States and
The Sackler Center for Computational Molecular and Materials Science, Tel Aviv University, Tel Aviv, Israel 69978*

Having already achieved near-unity quantum yields, with promising properties for light-emitting diode, lasing, and charge separation applications, colloidal core/shell quantum dots have great technological potential. The shell thickness and band alignment of the shell and core materials are known to influence the efficiency of these devices. In many such applications, a key to improving the efficiency requires a deep understanding of multiexcitonic states. Herein, we elucidate the shell thickness and band alignment dependencies of the biexciton Auger recombination lifetime for quasi-type-II CdSe/CdS and type-I CdSe/ZnS core/shell quantum dots. We find that the biexciton Auger recombination lifetime increases with the total nanocrystal volume for quasi-type-II CdSe/CdS core/shell quantum dots and is independent of the shell thickness for type-I CdSe/ZnS core/shell quantum dots. In order to perform these calculations and compute Auger recombination lifetimes, we developed a low-scaling approach based on the stochastic resolution of identity. The numerical approach provided a framework to study the scaling of the biexciton Auger recombination lifetimes in terms of the shell thickness dependencies of the exciton radii, Coulomb couplings, and density of final states in quasi-type-II CdSe/CdS and type-I CdSe/ZnS core/shell quantum dots.

The viability of many semiconductor nanomaterial-based applications relies upon the ability to control multiexcitonic states.^{1,2} For example, in typical nanomaterial-based lasers, generating population inversion requires two excitons in the nanosystem and, thus, the properties of the biexcitonic state determine, amongst other factors, the efficiency of the device.³⁻⁶ In fact, this is arguably the case for other applications such as light-emitting diodes^{3,7} and photocatalysts.⁸ Therefore, understanding the properties of the biexcitonic state and its decay channels is central to improving and further developing many light-induced applications.

One of the major decay channels of the biexcitonic state is Auger recombination (similar to exciton-exciton annihilation), which is a nonradiative process where an electron and hole recombine and transfer their energy to a nearby electron or hole in a Coulomb mediated process (Figure 1). Auger recombination is typically the dominant decay channel of biexcitons in semiconductor nanocrystals as it usually occurs on a sub-nanosecond timescale.

An aspect of biexciton Auger recombination that has drawn much attention over the years is that of how the rate of biexciton Auger recombination decay depends on the size of the nanocrystal.^{1,9-15} For single material colloidal quantum dots (QDs), the linear dependence of the biexciton lifetime with the QD volume has become known as the “universal volume scaling law.”¹⁰ Although the size of a single material colloidal QD is a knob that can be tuned to change the biexciton lifetime and, thus, the efficiency of nanodevices that rely on biexcitonic states, changing the size also drastically impacts single exciton properties. On the other hand, heterostructure nano-

materials have many experimentally tunable parameters, including relative size and band alignments between the individual component materials, that can be chosen to optimize the performance of nanodevices. For example, independently tuning the shell thickness and band alignment has resulted in heterostructure nanocrystals with near-unity quantum yields along with promising light-emitting diode and lasing properties.^{3,7,16-20} Interestingly, there have been multiple reports that the “universal volume scaling law” does not apply to core/shell QDs.^{7,21-26} Although, significant theoretical progress has been made,^{27,28} particularly on the impact of the sharpness of the core/shell interface on biexciton lifetimes,²⁹ a quantitatively accurate atomistic electronic structure method has not yet been developed for heterostructure nanomaterials due to the inherently large nature of heterostructure nanosystems and the steep scaling with system size of computing Auger recombination lifetimes.

With this difficulty in mind, we report an efficient, stochastic method for calculating biexciton Auger recombination (AR) lifetimes within Fermi’s golden rule suitable for large heterostructure nanosystems and apply it to elucidate the shell thickness dependence of AR in quasi-type-II CdSe/CdS and type-I CdSe/ZnS core/shell QDs (Figure 1). The stochastic approach, which also accounts for electron-hole correlations, reduces the scaling with the system size (N) of calculating AR lifetimes from $O(N^5)$ to $O(N^2)$ and predicts quantitatively accurate AR lifetimes in comparison to experiments. Additionally, the AR formalism predicts that adding a shell with a quasi-type-II band alignment (CdSe/CdS QDs) results in an increase in the AR lifetime, in agreement with previous experimental and theo-

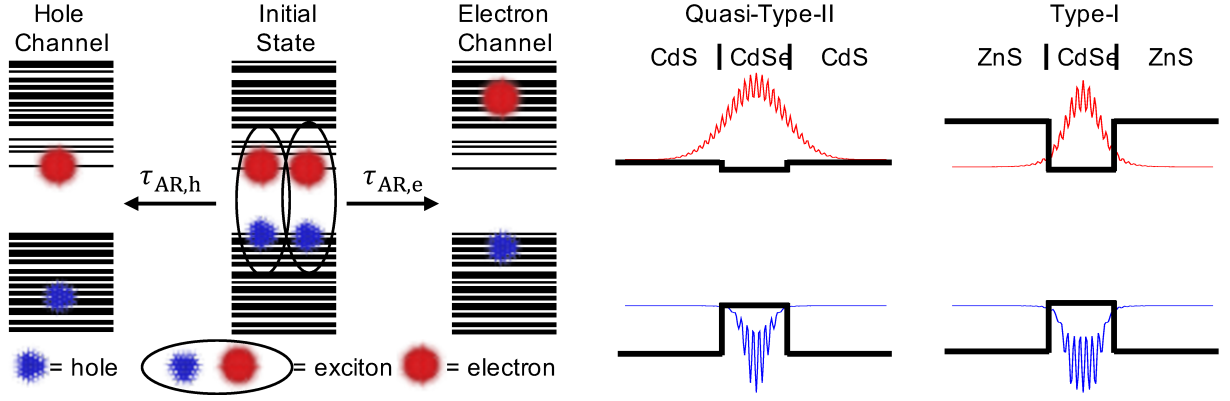


Figure 1. (A) Schematic of an Auger recombination event. The initial biexcitonic state is shown as two spatially uncorrelated excitonic states and the final states are shown as unbound electron–hole pairs. The hole (electron) channel on the left (right) shows the hole (electron) receiving a majority of the energy from the recombining exciton. (b) Schematic of the quasi–type–II nature of CdSe/CdS core/shell quantum dots and the type–I nature of CdSe/ZnS core/shell quantum dots. Projected electron (red) and hole (blue) probability densities are shown on top of the band alignment scheme to highlight the differences in electron localization between the two systems.

retical results,^{23,25,26,28,30} whereas the addition of a shell with a strictly type–I band alignment (CdSe/ZnS QDs) has little impact on the AR lifetime. Lastly, we explain the shell thickness dependencies of the AR lifetimes in terms of the size dependencies of the root–mean–square exciton radius, Coulomb coupling, and density of final states in quasi–type–II CdSe/CdS and type–I CdSe/ZnS core/shell QDs.

AR is a Coulomb mediated process for which an initial biexcitonic state ($|B\rangle$) of energy E_B decays into a final excitonic state ($|S\rangle$) of energy E_S via Coulomb scattering (V). An AR lifetime (τ_{AR}) for a nanomaterial can be calculated using Fermi’s golden rule where we average over thermally distributed initial biexcitonic states and

sum over all final decay channels into single excitonic states:

$$\tau_{AR}^{-1} = \sum_B \frac{e^{-\beta E_B}}{Z_B} \left[\frac{2\pi}{\hbar} \sum_S |\langle B|V|S\rangle|^2 \delta(E_B - E_S) \right] \quad (1)$$

In the above, the delta function ($\delta(E_B - E_S)$) enforces energy conservation between the initial and final states and the partition function ($Z_B = \sum_B e^{-\beta E_B}$) is for the initial biexcitonic states (we assume Boltzmann statistics for biexcitons). Utilizing the interacting framework, previously developed by Philbin and Rabani,¹⁴ a deterministic calculation of an AR lifetime can be performed using

$$\begin{aligned} \tau_{AR}^{-1} = & \frac{2\pi}{\hbar Z_B} \sum_B e^{-\beta E_B} \sum_{a,i} \left| \sum_{b,c,k} c_{b,i}^B c_{c,k}^B V_{abck} \right|^2 \delta(E_B - \varepsilon_a + \varepsilon_i) \\ & + \frac{2\pi}{\hbar Z_B} \sum_B e^{-\beta E_B} \sum_{a,i} \left| \sum_{j,c,k} c_{a,j}^B c_{c,k}^B V_{ijck} \right|^2 \delta(E_B - \varepsilon_a + \varepsilon_i), \end{aligned} \quad (2)$$

where the indices a, b, c, \dots refer to the electron (unoccupied) states, i, j, k, \dots refer to the hole (occupied) states with corresponding energies ε_a and ε_i , r, s, u, \dots are general indices, and V_{rsut} is the Coulomb coupling given by

$$V_{rsut} = \iint \frac{\phi_r(\mathbf{r}) \phi_s(\mathbf{r}) \phi_u(\mathbf{r}') \phi_t(\mathbf{r}')}{|\mathbf{r} - \mathbf{r}'|} d^3\mathbf{r} d^3\mathbf{r}'. \quad (3)$$

The coefficients ($c_{c,k}^B$) in Eq. (2) are determined by solving the Bethe–Salpeter equation.³¹ For more details, please consult Ref. 14. The above formalism includes

spatial correlations within the electron–hole pairs but ignores them between the two excitons³² and in the final electron–hole pair (Figure 1). This approximation for the final state is valid in a majority of nanomaterials as the energy of the final electron–hole pair is approximately twice the optical gap, which is well above the typical exciton binding energy in all semiconductor nanomaterials.³³ In other words, the criteria for being able to approximate the final high energy excitonic state as an uncorrelated electron–hole pair instead of a Wannier or Frenkel exciton

is that $E_{\text{opt}} \gg E_b$, where E_{opt} is the optical gap and E_b is the exciton binding energy. It was previously shown that this interacting (i.e. exciton-based) AR formalism (Eq. (2)) predicts quantitatively accurate AR lifetimes for both single material QDs and nanorods.¹⁴ On the other hand, noninteracting formalisms that ignore all electron-hole correlations in the initial biexcitonic state predict neither accurate AR lifetimes nor the scaling of the lifetimes with respect to QD volume except for QDs in the very strong confinement regime³⁴ — highlighting the importance of electron-hole correlations and the resulting Wannier exciton formation in semiconductor nanomaterials.¹⁴

The main drawback of the exciton-based (interacting) AR formalism for calculating AR lifetimes (Eq. (2)) is the computational cost. Formally, the steepest scaling involved in Eq. (2) is diagonalization of the Bethe-Salpeter Hamiltonian to obtain the coefficients ($c_{c,k}^B$), which formally scales as $O(N^6)$. However, in practice this takes less than 10% of the computational time for nanomaterials with $\leq 10,000$ atoms because only a few low-lying energy states are required in order to calculate the AR lifetime due to the Boltzmann factors in Eq. (2). The majority of the computational time is spent on calculating all of the Coulomb matrix elements, V_{abck} and V_{ijck} , that couple the initial biexcitonic states with the final electron-hole pairs. The number of Coulomb matrix elements that must be calculated scales as $O(N_{e,\text{final}}N_e^2N_h + N_{h,\text{final}}N_h^2N_e) \sim O(N^4)$, where $N_{e(h),\text{final}}$ is the number of high energy final electron (hole) states and $N_{e(h)}$ is the number of band-edge

electron (hole) states, and the cost of calculating each Coulomb matrix element scales with the number of real-space grid points (N_{grid}) as $O(N_{\text{grid}} \ln N_{\text{grid}})$ to give the overall scaling of $O(N^5)$. This limits the application of Eq. (2) to relatively small systems ($< 1,000$ atoms).

To reduce the computational effort and scaling of the rate limiting step, we employ a plane-wave stochastic representation of the Coulomb operator:³⁵

$$V_{rsut} \approx \left\langle R_{rs}^\zeta R_{ut}^\zeta \right\rangle_\zeta \quad (4)$$

where the notation $\langle \dots \rangle_\zeta$ denotes an average over N_s stochastic orbitals (defined below),

$$R_{rs}^\zeta = \int \phi_r^*(\mathbf{r}) \phi_s^*(\mathbf{r}) \theta^\zeta(\mathbf{r}) d^3\mathbf{r}, \quad (5)$$

and $\theta^\zeta(\mathbf{r})$ is a stochastic representation of the Coulomb integral given by

$$\theta^\zeta(\mathbf{r}) = \frac{1}{(2\pi)^3} \int d\mathbf{k} \sqrt{\tilde{u}_C(\mathbf{k})} e^{i\varphi(\mathbf{k})} e^{i\mathbf{k}\cdot\mathbf{r}}. \quad (6)$$

In the above equations, $\varphi(\mathbf{k})$ is a random phase between 0 and 2π at each k -space grid point, $\tilde{u}_C(\mathbf{k}) = \frac{4\pi}{k^2}$ is the Fourier transform of the Coulomb potential, and the stochastic orbitals ($\theta^\zeta(\mathbf{r})$) are indexed by ζ . By inserting Eq. (4) into Eq. (2), we obtain

$$\begin{aligned} \tau_{\text{AR}}^{-1} &= \tau_{\text{AR,e}}^{-1} + \tau_{\text{AR,h}}^{-1} \\ \tau_{\text{AR,e}}^{-1} &= \frac{2\pi}{\hbar Z_B} \sum_B e^{-\beta E_B} \sum_{a,i} \left\langle \sum_b c_{b,i}^B R_{ab}^{\zeta'} \sum_{c,k} c_{c,k}^B R_{ck}^{\zeta'} \right\rangle_{\zeta'}^* \left\langle \sum_b c_{b,i}^B R_{ab}^\zeta \sum_{c,k} c_{c,k}^B R_{ck}^\zeta \right\rangle_\zeta \delta(E_B - \varepsilon_a + \varepsilon_i) \\ \tau_{\text{AR,h}}^{-1} &= \frac{2\pi}{\hbar Z_B} \sum_B e^{-\beta E_B} \sum_{a,i} \left\langle \sum_j c_{a,j}^B R_{ij}^{\zeta'} \sum_{c,k} c_{c,k}^B R_{ck}^{\zeta'} \right\rangle_{\zeta'}^* \left\langle \sum_j c_{a,j}^B R_{ij}^\zeta \sum_{c,k} c_{c,k}^B R_{ck}^\zeta \right\rangle_\zeta \delta(E_B - \varepsilon_a + \varepsilon_i), \end{aligned} \quad (7)$$

where $\tau_{\text{AR,e}}$ and $\tau_{\text{AR,h}}$ are the lifetimes for the electron and hole channels, respectively (Figure 1). The calculation of an AR lifetime using Eq. (7) scales as $O(N^3)$.

To further reduce the computational scaling and complexity, we utilize the stochastic resolution of the identity^{36,37} within the subspace of the final high energy electron and hole parts of the Hamiltonian. In simpler terms,

we sample the final high energy electron and hole states in order to reduce the scaling with number of final excitonic states. Thus, we arrive at a general expression for calculating AR lifetimes of semiconductor nanomaterials using an efficient, doubly stochastic formulation of the interacting (exciton-based) AR formalism

$$\begin{aligned} \tau_{\text{AR}}^{-1} &= \tau_{\text{AR,e}}^{-1} + \tau_{\text{AR,h}}^{-1} \\ \tau_{\text{AR,e}}^{-1} &= \frac{2\pi}{\hbar Z_B} \sum_B e^{-\beta E_B} \left\langle \left\langle \sum_b c_{b,i^A}^B R_{\theta^A b}^{\zeta'} \sum_{c,k} c_{c,k}^B R_{ck}^{\zeta'} \right\rangle_{\zeta'}^* \left\langle \sum_b c_{b,i^A}^B R_{\theta^A b}^\zeta \sum_{c,k} c_{c,k}^B R_{ck}^\zeta \right\rangle_\zeta \right\rangle_A \end{aligned} \quad (8)$$

$$\tau_{\text{AR,h}}^{-1} = \frac{2\pi}{\hbar Z_B} \sum_B e^{-\beta E_B} \left\langle \left\langle \sum_j c_{a^I,j}^B R_{\theta^I,j}^{\zeta'} \sum_{c,k} c_{c,k}^B R_{c,k}^{\zeta'} \right\rangle_{\zeta'}^* \left\langle \sum_j c_{a^I,j}^B R_{\theta^I,j}^{\zeta} \sum_{c,k} c_{c,k}^B R_{c,k}^{\zeta} \right\rangle_{\zeta} \right\rangle_I,$$

where the indices θ^A , i^A and a^I , θ^I in Eq. (8) are sampled final states from the complete set of single excitonic states (a , i pairs) in Eq. (7). Energy conservation in Eq. (8) has been taken into account when forming the stochastic orbitals that sample the final excitonic states, namely, we only sample states that preserve energy. The computational cost of Eq. (8) is $O(N^2)$. This scaling does assume that the number of stochastic orbitals required to properly converge the calculations does not increase with the system size, which has shown to be true for a variety of electronic structure methods.^{36–40} Another beneficial feature of Eq. (8) is that it is embarrassingly parallel over all sets of stochastic orbitals. The speedup that arises from using Eq. (8) instead of Eq. (2) ranges from ~ 5 for QDs with 1,000 atoms to greater than 1,000 for QDs with 10,000 atoms. This speedup made the study of the large core/shell QDs presented in the remainder of this Letter possible. The Supporting Information contains more information on the derivation, implementation and computational cost of the above equations and similar expressions for the noninteracting, free carrier–based formalism.

We have implemented the above equations using the semi–empirical pseudopotential method to model the electron and hole states.^{34,41–43} We utilized the filter–diagonalization technique^{44,45} to selectively calculate the low energy electron and hole states required to accurately describe the excitonic states that compose the initial biexcitonic state and the high energy electron and hole states that satisfy energy conservation. The Bethe–Salpeter equation³¹ was solved within the static screening approximation. And all electronic structure calculations were performed using the minimum energy atomic configuration obtained via molecular dynamic minimization⁴⁶ of the heterostructure QDs. This computational scheme has been shown to predict quantitatively accurate single excitonic properties (e.g. optical gap and emission polarizations) and accurately takes into account the important effects of strain in heterostructure nanomaterials that arise from the lattice mismatch between core and shell materials.^{18,19}

Figure 2 displays the calculated AR lifetimes using Eq. (8) for the $d_{\text{core}} = 3.8$ nm CdSe/CdS QDs along with the experimentally measured AR lifetimes²⁶ and AR lifetimes calculated using a noninteracting, free carrier–based formalism.³⁴ Quantitative agreement with the experimental measurements on similarly sized CdSe/CdS QDs is observed when Eq. (8) is used. It is important to note that all of the core/shell QDs studied in this work have sharp core/shell interfaces.²⁵ In other words, there is no alloying region between the core and shell materials that is known to have important consequences on AR

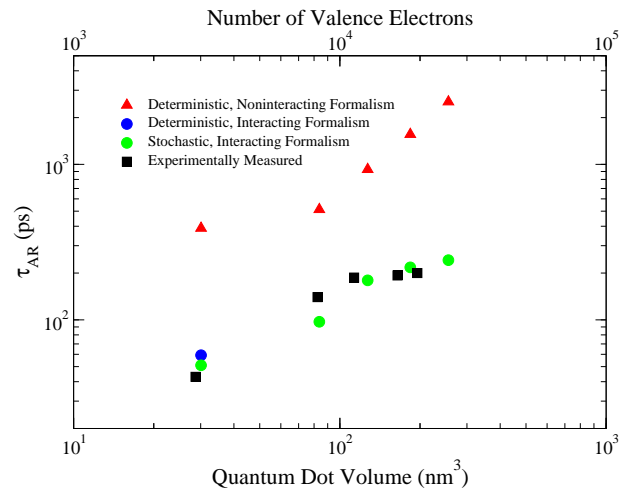


Figure 2. Comparison of Auger recombination lifetimes (τ_{AR}) that have been experimentally measured²⁶ (black), calculated using the deterministic interacting formalism (blue), stochastic formulation of the interacting formalism (green), and the deterministic formulation of the noninteracting formalism (red) of CdSe/CdS core/shell quantum dots with a CdSe core diameter of 3.8 nm and varying number of CdS shell monolayers.

lifetimes.^{21,27,29} The quantitative agreement shows the generality of the interacting (exciton–based) AR formalism for predicting quantitatively accurate AR lifetimes in nanomaterials. It is worthwhile to note that a noninteracting (free–carrier based) AR formalism predicts incorrect AR lifetimes in core/shell QDs, similar to the single material case.

Figure 3 summarizes a main result of this work. The top panel of Figure 3 compares calculated AR lifetimes for CdSe cores with a diameter of 2.2 nm ($d_{\text{core}} = 2.2$ nm) as a function of the number of shell monolayers (MLs) for both CdS and ZnS from 0 MLs to up to 8 MLs. This constitutes a range of nanocrystal sizes from approximately 200 atoms ($V_{\text{QD}} \sim 5$ nm³) to nearly 10,000 atoms ($V_{\text{QD}} \sim 350$ nm³). Figure 3 highlights the dramatically different impact that growing a quasi–type–II shell (CdS) has on the AR lifetime compared to growing a type–I (ZnS) shell on a QD core (CdSe). Specifically, the addition of more and more CdS MLs leads to the AR lifetime increasing from ~ 5 ps for the 0 ML QD to ~ 35 ps and ~ 150 ps upon addition of 4 and 8 MLs of CdS, respectively, for the $d_{\text{core}} = 2.2$ nm CdSe QD core. On the other hand, for the same CdSe core, the addition of 4 and 8 MLs of ZnS does not lead to an increase in the AR lifetime.

In order to understand the vastly different shell thickness dependencies of the AR lifetimes between CdSe/CdS

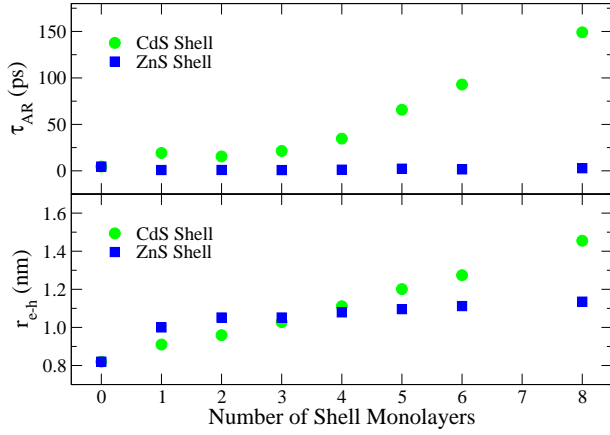


Figure 3. Auger recombination lifetimes (top) and root-mean-square exciton radii ($r_{e-h} = \sqrt{\langle r_{e-h}^2 \rangle}$), bottom) of CdSe/CdS (green) and CdSe/ZnS (blue) core/shell quantum dots as a function of the number CdS and ZnS shell monolayers, respectively, for a CdSe core diameter of 2.2 nm.

and CdSe/ZnS QDs, we plot the root-mean-square exciton radius ($\sqrt{\langle r_{e-h}^2 \rangle}$ where r_{e-h} is the electron-hole radial coordinate)⁴⁷ as a function of the number of shell MLs for both series of core/shell QDs in the bottom panel of Figure 3. For CdSe/CdS QDs, the root-mean-square exciton radius systematically increases with the number of shell MLs. On the other hand, for CdSe/ZnS QDs there is an increase upon adding the first ZnS layer, but then the addition of more and more ZnS MLs barely changes the root-mean-square exciton radius. Specifically, the root-mean-square exciton radius increases from 1.11 nm to 1.46 nm upon going from 4 MLs to 8 MLs of CdS but only increases from 1.08 nm to 1.14 nm upon going from 4 MLs to 8 MLs of ZnS for the same $d_{core} = 2.2$ nm CdSe core (bottom panel of Figure 3).

These different dependencies of the AR lifetime and root-mean-square exciton radius with shell thickness are a direct consequence of the quasi-type-II^{26,48} and type-I nature of the CdS and ZnS shells, respectively. Figure 4 shows the hole and electron carrier densities of the lowest energy excitonic state (i.e. electron-hole interactions have been included) projected onto the x -axis of the core/shell QDs for the $d_{core} = 2.2$ nm CdSe QD cores with 0 MLs, 4 MLs and 8 MLs of shell. For CdSe/CdS (left panels of Figure 4), the quasi-type-II nature can be observed as the projected hole density remains confined to the CdSe core for all shell thicknesses while the electron density continuously spreads out into the CdS shell. In contrast, both the hole and electron densities remain confined to the CdSe core in CdSe/ZnS core/shell QDs, highlighting the type-I band alignment of CdSe/ZnS core/shell QDs (right panels of Figure 4). The impact of the electron spreading out into the CdS shell and, thus, increasing the root-mean-square exciton radius in larger CdS shell nanocrystals leads to a decrease in the Coulomb coupling involved in AR calculations. This result can be understood by noting that

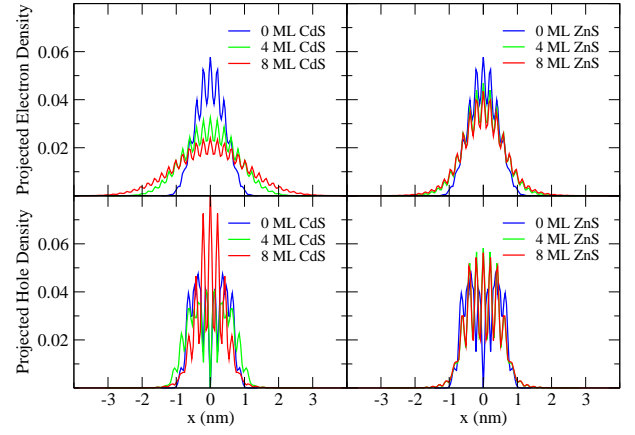


Figure 4. Hole and electron carrier densities of the lowest energy excitonic state for a series of shell thicknesses for CdSe/CdS and CdSe/ZnS core/shell QDs with a CdSe core diameter of 2.2 nm.

the larger the electron and hole wavefunctions overlap the larger the Coulomb matrix elements, as the product $\phi_c(\mathbf{r}')\phi_k(\mathbf{r}')$ where $\phi_c(\mathbf{r}')$ and $\phi_k(\mathbf{r}')$ are wavefunctions for an initial electron and hole, respectively, arises in the Coulomb coupling (Eq. (3)).

The type-I band alignment of CdSe/ZnS core/shell QDs results in the addition of ZnS MLs barely changing the root-mean-square exciton radius and not increasing the AR lifetime. Surprisingly, the AR lifetimes for all CdSe/ZnS core/shell QDs are slightly shorter, with lifetimes of ~ 2 ps, compared to the ~ 5 ps AR lifetime for the bare CdSe core (Figure 3). To elucidate whether or not the compressive strain of the ZnS shell causes the decrease of the AR lifetime, we performed AR lifetimes calculations on strained CdSe cores. Specifically, we performed molecular dynamics based structural minimizations with ZnS shells and then removed the ZnS shells before performing the electronic structure calculations. This procedure resulted in compressively strained CdSe QDs,¹⁹ where the degree of compressive strain was related to the number of ZnS MLs that were present during molecular dynamics minimization. Our calculations on this series of CdSe QDs show that the AR lifetime decreases from ~ 5 ps to ~ 2 ps upon increasing the strain on the CdSe QD (Table SX). Interestingly, the AR lifetime decreasing by $\sim 250\%$ upon adding strain to the CdSe QD is much greater than would be expected due to just a volumetric change as the compressive strain only changes the CdSe QD volume by $\sim 10\%$. We were able to trace the decrease of the AR lifetime to a decrease in the hole channel AR lifetime. Furthermore, the decrease of the hole channel AR lifetime was caused by an increase in the average Coulomb coupling matrix elements (V_{ijck}) of the hole channel and not by any substantial changes in the density of final states (Table SX). Thus, it appears that the hole channel is more sensitive to stress induced structural changes. And this suggests it is worthwhile to perform more comprehensive studies on the impact of

strain on AR lifetimes, as strain may be playing a role in other nonmonotonic dependencies of AR in core/shell nanomaterials.²⁴ That being said, we do note that this is a rather small change of the AR lifetime and experimental confirmation of this decrease in the AR lifetime upon ZnS shell growth on QDs would likely be impeded by inhomogeneous broadening and alloying of the core/shell interface. A more elaborate discussion of the decrease of the AR lifetime upon the addition of a ZnS shell and its relation to strain is given in the Supporting Information.

The goals of this study were to elucidate how biexciton Auger recombination in colloidal core/shell QDs can be accurately modeled and efficiently computed, and to uncover some of the underlying physics of excitons and biexcitons in core/shell QDs by testing different approximations. In order to achieve these goals, we developed a stochastic computational scheme for calculating the non-radiative decay rate of biexcitonic states. This efficient, stochastic method for calculating Auger recombination lifetimes presented in this Letter is general and can be used for any confined nanomaterial. We also utilized this efficient method for calculating quantitatively accurate

biexciton Auger recombination lifetimes within an interacting (exciton-based) formalism to elucidate the different impact of growing quasi-type-II (CdS) and type-I (ZnS) shells on QD cores (CdSe). Specifically, we showed that the Auger recombination lifetime monotonically increases as the number of quasi-type-II shell monolayers increases whereas the Auger recombination lifetime is mainly unchanged upon the addition of type-I shells.

ACKNOWLEDGMENTS

E.R. acknowledges support from the Department of Energy, Photonics at Thermodynamic Limits Energy Frontier Research Center, under Grant No. de-sc0019140. We also acknowledge the University of California Lab Fee Research Program (Grant LFR-17-477237) and the National Energy Research Scientific Computing Center (NERSC), a U.S. Department of Energy Office of Science User Facility operated under Contract No. DE-AC02-05CH11231.

-
- * jphilbin@berkeley.edu
 † eran.rabani@berkeley.edu
- ¹ V. I. Klimov, A. A. Mikhailovsky, D. W. McBranch, C. A. Leatherdale, and M. G. Bawendi, *Science* **287**, 1011 (2000).
 - ² V. I. Klimov, *Annual Review of Condensed Matter Physics* **5**, 285 (2014).
 - ³ V. I. Klimov, S. S. a. Ivanov, J. Nanda, M. Achermann, I. Bezel, J. a. J. McGuire, and A. Piryatinski, *Nature* **447**, 441 (2007).
 - ⁴ C. She, I. Fedin, D. S. Dolzhenkov, P. D. Dahlberg, G. S. Engel, R. D. Schaller, and D. V. Talapin, *ACS Nano* **9**, 9475 (2015).
 - ⁵ J. Lim, Y. S. Park, and V. I. Klimov, *Nature Materials* **17**, 42 (2018).
 - ⁶ J. Roh, Y. S. Park, J. Lim, and V. I. Klimov, *Nature Communications* **11**, 271 (2020).
 - ⁷ W. K. Bae, Y.-S. Park, J. Lim, D. Lee, L. a. Padilha, H. McDaniel, I. Robel, C. Lee, J. M. Pietryga, and V. I. Klimov, *Nature Communications* **4**, 2661 (2013).
 - ⁸ Y. Ben-Shahar, J. P. Philbin, F. Scotognella, L. Ganzar, G. Cerullo, E. Rabani, and U. Banin, *Nano Letters* **18**, 5211 (2018).
 - ⁹ V. I. Klimov, J. A. McGuire, R. D. Schaller, and V. I. Rupasov, *Physical Review B* **77**, 195324 (2008).
 - ¹⁰ I. Robel, R. Gresback, U. Kortshagen, R. D. Schaller, and V. I. Klimov, *Physical Review Letters* **102**, 177404 (2009).
 - ¹¹ L. A. Padilha, J. T. Stewart, R. L. Sandberg, W. K. Bae, W.-k. Koh, J. M. Pietryga, and V. I. Klimov, *Nano Letters* **13**, 1092 (2013).
 - ¹² R. Vaxenburg, A. Rodina, A. Shabaev, E. Lifshitz, and A. L. Efros, *Nano Letters* **15**, 2092 (2015).
 - ¹³ Q. Li and T. Lian, *Nano Letters* **17**, 3152 (2017).
 - ¹⁴ J. P. Philbin and E. Rabani, *Nano Letters* **18**, 7889 (2018).
 - ¹⁵ Q. Li, Y. Yang, W. Que, and T. Lian, *Nano Letters* **19**, 5620 (2019).
 - ¹⁶ F. García-Santamaría, Y. Chen, J. Vela, R. D. Schaller, J. A. Hollingsworth, and V. I. Klimov, *Nano Letters* **9**, 3482 (2009).
 - ¹⁷ Q. Li, J. Zhao, V. P. Chauhan, J. Cui, C. Wong, D. K. Harris, H. Wei, H. S. Han, D. Fukumura, R. K. Jain, and M. G. Bawendi, *Nature Materials* **12**, 445 (2013).
 - ¹⁸ I. Hadar, J. P. Philbin, Y. E. Panfil, S. Neyshtadt, I. Lieberman, H. Eshet, S. Lazar, E. Rabani, and U. Banin, *Nano Letters* **17**, 2524 (2017).
 - ¹⁹ A. Hazarika, I. Fedin, L. Hong, J. Guo, V. Srivastava, W. Cho, I. Coropceanu, J. Portner, B. T. Diroll, J. P. Philbin, E. Rabani, R. Klie, and D. V. Talapin, *Journal of the American Chemical Society* **141**, 13487 (2019).
 - ²⁰ D. A. Hanifi, N. D. Bronstein, B. A. Koscher, Z. Nett, J. K. Swabeck, K. Takano, A. M. Schwartzberg, L. Maserati, K. Vandewal, Y. van de Burgt, A. Salleo, and A. P. Alivisatos, *Science* **363**, 1199 (2019).
 - ²¹ F. García-Santamaría, S. Brovelli, R. Viswanatha, J. A. Hollingsworth, H. Htoon, S. A. Crooker, and V. I. Klimov, *Nano Letters* **11**, 687 (2011).
 - ²² C. Javaux, B. Mahler, B. Dubertret, A. Shabaev, A. V. Rodina, A. L. Efros, D. R. Yakovlev, F. Liu, M. Bayer, G. Camps, L. Biadala, S. Buil, X. Quelin, and J.-P. J.-P. Hermier, *Nature Nanotechnology* **8**, 206 (2013).
 - ²³ R. Vaxenburg, A. Rodina, E. Lifshitz, and A. L. Efros, *Nano Letters* **16**, 2503 (2016).
 - ²⁴ M. Pelton, J. J. Andrews, I. Fedin, D. V. Talapin, H. Leng, and S. K. O’Leary, *Nano Letters* **17**, 6900 (2017).
 - ²⁵ L. Zhang, H. Li, C. Liao, H. Yang, R. Xu, X. Jiang, M. Xiao, C. Lu, Y. Cui, and J. Zhang, *Journal of Physical Chemistry C* **122**, 25059 (2018).
 - ²⁶ D. Kong, Y. Jia, Y. Ren, Z. Xie, K. Wu, and T. Lian, *Journal of Physical Chemistry C* **122**, 14091 (2018).

- ²⁷ A. Jain, O. Voznyy, S. Hoogland, M. Korzukinski, P. Hawrylak, and E. H. Sargent, *Nano Letters* **16**, 6491 (2016).
- ²⁸ A. L. Kaledin, D. Kong, K. Wu, T. Lian, and D. G. Musaev, *Journal of Physical Chemistry C* **122**, 18742 (2018).
- ²⁹ G. E. Cragg and A. L. Efros, *Nano Letters* **10**, 313 (2010).
- ³⁰ Y. S. Park, W. K. Bae, L. A. Padilha, J. M. Pietryga, and V. I. Klimov, *Nano Letters* **14**, 396 (2014).
- ³¹ M. Rohlfing and S. G. Louie, *Physical Review B* **62**, 4927 (2000).
- ³² S. Refaely-Abramson, F. H. Da Jornada, S. G. Louie, and J. B. Neaton, *Physical Review Letters* **119**, 267401 (2017).
- ³³ F. Wang, Y. Wu, M. S. Hybertsen, and T. F. Heinz, *Physical Review B* **73**, 245424 (2006).
- ³⁴ L.-W. Wang, M. Califano, A. Zunger, and A. Franceschetti, *Physical Review Letters* **91**, 056404 (2003).
- ³⁵ D. Neuhauser, E. Rabani, Y. Cytter, and R. Baer, *Journal of Physical Chemistry A* **120**, 3071 (2016).
- ³⁶ T. Y. Takeshita, W. A. D. Jong, D. Neuhauser, R. Baer, and E. Rabani, *Journal of Chemical Theory and Computation* **13**, 4605 (2017).
- ³⁷ W. Dou, T. Y. Takeshita, M. Chen, R. Baer, D. Neuhauser, and E. Rabani, *Journal of Chemical Theory and Computation* **15**, 6703 (2019).
- ³⁸ R. Baer and E. Rabani, *Nano Letters* **12**, 2123 (2012).
- ³⁹ R. Baer, D. Neuhauser, and E. Rabani, *Physical Review Letters* **111**, 106402 (2013), arXiv:1304.4053.
- ⁴⁰ D. Neuhauser, Y. Gao, C. Arntsen, C. Karshenas, E. Rabani, and R. Baer, *Physical Review Letters* **113**, 076402 (2014).
- ⁴¹ L. W. Wang and A. Zunger, *The Journal of Physical Chemistry* **98**, 2158 (1994).
- ⁴² L.-W. Wang and A. Zunger, *Physical Review B* **53**, 9579 (1996).
- ⁴³ E. Rabani, B. Hetenyi, B. J. Berne, and L. E. Brus, *The Journal of Chemical Physics* **110**, 5355 (1999).
- ⁴⁴ M. R. Wall and D. Neuhauser, *The Journal of Chemical Physics* **102**, 8011 (1995).
- ⁴⁵ S. Toledo and E. Rabani, *Journal of Computational Physics* **180**, 256 (2002).
- ⁴⁶ X. W. Zhou, D. K. Ward, J. E. Martin, F. B. Van Swol, J. L. Cruz-Campa, and D. Zubia, *Physical Review B* **88**, 085309 (2013).
- ⁴⁷ A. Brumberg, S. M. Harvey, J. P. Philbin, B. T. Diroll, S. A. Crooker, M. R. Wasielewski, E. Rabani, and R. D. Schaller, *ACS Nano* **13**, 8589 (2019).
- ⁴⁸ H. Eshet, M. Grünwald, and E. Rabani, *Nano Letters* **13**, 5880 (2013), arXiv:arXiv:1307.6097v2.